The 2009 IEEE/RSJ International Conference on
Intelligent Robots and Systems
October 11-15, 2009 St. Louis, USA

Improvement of Simulation Model and Development of Control Mechanism of force direction for a Flying Robot with Cyclogyro Wing

Yoshiyuki Higashi, Kazuo Tanaka, Hiroshi Ohtake and Hua O. Wang

Abstract— **This paper discusses the improvement of the simulation model and the development of the new mechanism for flight control of a flying robot with the cyclogyro wing. In past study, we focused high maneuverability of the flying robots with the cyclogyro wing, whose rotor had rotation along horizontal axis, and developed some prototypes. The simulation model was also constructed based on the pressure of air. However the Reynolds number was not considered in the constructed simulation model. As a results, the model's accuracy was not enough. On the other hand, the control mechanism for the flight of cyclogyro wing is not yet developed. In this paper, the simulation model is improved by considering the cyclogyro's Reynolds number. The utility of the improved simulation model is verified by comparing simulation results with experimental results. Moreover the new mechanism is suggested for the flight control by controlling the generated force direction. The prototype of the new mechanism is developed and validated by the experiment.**

I. INTRODACTION

Nowadays, several flying robots are studied on their information gathering ability and high maneuverability. These studies are categorized into the investigation using existing aircraft such as the helicopter and the development of new flight mechanism like the flutter robot. The former attaches importance to the guidance and the control of aircraft [1][2][3]. On the other hand, the latter is focused on the development of the new thruster and the mechanism for flight control [4][5].

With respect to mechanism of generating lift forces, a unique mechanism, named cyclogyro, was proposed in 1930's. An airplane with the mechanism was designed at the time. Fig. 1 shows an image picture of cyclogyro-based airplane planned in 1930's. The cyclogyro (or cyclogyre) is an airplane propelled and given lift by horizontal assemblies of rotating wings. According to the web [6], very few prototypes were built, and those that were constructed were completely unsuccessful. The essential principle is that the angle of attack of the rotating wings is altered as they go round, allowing the lift/thrust vector to be altered. This allows the airplane to rise vertically, hover, and even go backwards with various attitudes. Thus, cyclogyro-based flying robot has possibility of being a high maneuverability MAV. This advantage in the flight ability is brought out in the disaster site. To the best of our knowledge, nobody has proposed effective and practical mechanism of altering angles of attack. Thus, there is no record of any successful flights although machines of this type have been designed by some companies.

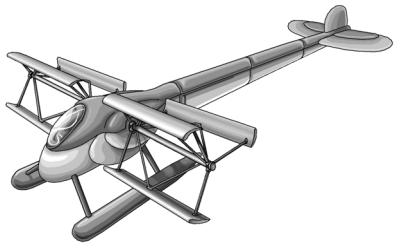

Fig. 1. An image picture of cyclogyro-based airplane planned in 1930's.

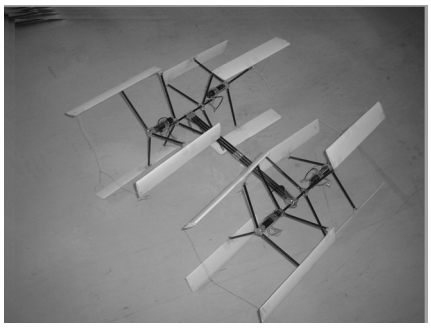

Fig. 2. Cyclogyro-based flying robot developed in [7].

In [7], we proposed a new variable attack angle mechanism that is quite simple and effective, and developed a flying robot with the mechanism. In addition, we demonstrated in some experiments that the change of attack angle provided enough lift force to fly if the parameters (the wing span, the number of wings and the eccentric distance) are appropriately designed. However, due to parameter selection based on experiments, we needed to build another robot, whenever a design parameter was changed. Hence, just only two or three selections for each design parameter were considered in [7]. The approach is quite inefficient from the development effort points of view.

For overcoming this problem, the simulation model composed three models called angle of attack model, lift force

Y. Higashi, K. Tanaka and H. Ohtake is with the Department of Mechanical Engineering and Intelligent Systems, The University of Electro-Communications, Chofu, Tokyo 182-8585 Japan y.higashi@rc.mce.uec.ac.jp, ktanaka@mce.uec.ac.jp, hohtake@mce.uec.ac.jp

H. O. Wang is with Department of Mechanical Engineering, Boston University, Boston, MA 02215 USA wangh@bu.edu

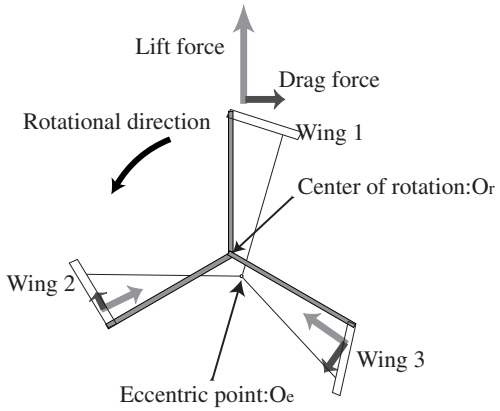

Fig. 3. Variable attack angle mechanism (overview).

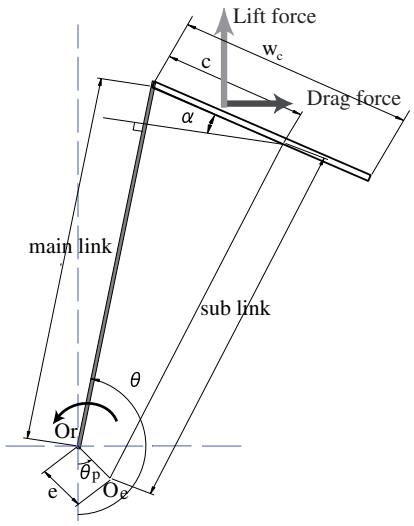

Fig. 4. Variable attack angle mechanism (detailed view).

model and power model was developed in [8]. But this lift force model does not contain the wing characteristic. Therefore, the model calculates only the lift force using only the force that air pushes the wing. As a result, the constructed lift force model had some error between the simulation results and the experimental results.

On the other hand, the greatest merit of the cyclogyro wing is its maneuverability, that is, it can flight with various attitudes. However, the mechanism of the flight control for the cyclogyro wing is not yet developed. Thus its rotor could not change the direction of the generated force, and it could not control the attitude of the flying robot.

In this paper, to improve the accuracy of the simulation model, we reconstruct the lift force model by considering the cyclogyro wing's Reynolds number and the aerodynamic characteristic of wings. The utility of the new simulation model is validated by comparing the new simulation model with previous results and experimental results. Moreover, the new mechanism for the control of the generated force direction is developed. Its validity is evaluated by the experiment with prototype.

II. FLYING ROBOT WITH VARIABLE ATTACK ANGLE MECHANISM

Fig. 2 shows the cyclogyro-based flying robot developed in [7]. Four sets of cyclogyro wings (rotated by four motors) are located to cancel each anti-torque generated by each rotor. Fig. 3 shows one set of cyclogyro wings (i.e., the variable attack angle mechanism) shown in Fig. 2. Fig. 4 shows the detail of the variable attack angle mechanism that consists of two different rotational points (the rotational center O_r and the eccentric point O_e) and the wing. e is the distance (eccentric distance) between O_r and O_e. w_c is the wing chord, θ is the angle between the horizontal axis and the main link. The eccentric angle θ_p is the angle between the vertical axis and the O_r-O_e line. α is the attack angle, that is, the angle between rotational direction and wing chord. The attack angle α of the wing can be changed by the double crank mechanism with two different rotational points. Design parameters of the robot are summarized below.

- main-link length : l_m [mm]
- sub-link length : l_s [mm]
- eccentric distance : e [mm]
- eccentric angle : θ_p [deg.]
- distance between links : c [mm]
- wing chord : w_c [mm]
- wing span : b [mm]
- the number of wings : n

The eccentric distance e and the eccentric angle θ_p are peculiar parameters in the variable attack angle mechanism. e and θ_p affect the amplitude of the attack angle and the direction of aerodynamic force vector, respectively. Therefore, flying direction of the robot can be controlled by manipulating θ_p. Since the wing area S can be calculated from the wing span and the wing chord, the wing area is excluded from the design parameters.

Fig. 5 shows the flow of the simulation model. The simulation model constructed here consists of three parts. The first part is an "angle of attack model" that calculates the attack angle $\alpha(\theta)$ corresponding to the rotational angle θ, i.e., the pitching motion of each wing. The second part is a "lift force model" that calculates the lift force corresponding to the attack angle calculated in the first part. The third part is a "power model" for calculating electric power consumption of motors caused by drag forces obtained in the second part. In the next section, the lift force model is reconstructed for improvement of the accuracy.

III. IMPROVEMENT OF LIFT FORCE SIMULATION MODEL

In the lift force model of the previous simulation model in [8], the lift L and drag D generated by the wing were calculated based on the pressure of air as

$$L(\theta) = \frac{1}{2}\rho v^2 S \sin\alpha(\theta)\cos\alpha, \quad (1)$$

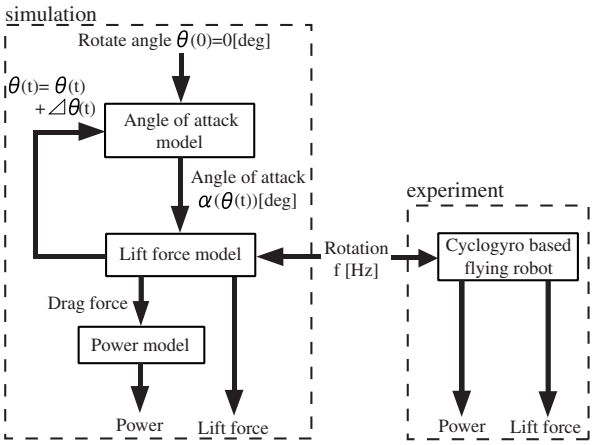

Fig. 5. Simulation model flow.

$$D(\theta) = \frac{1}{2}\rho v^2 S \sin\alpha(\theta)\sin\alpha. \quad (2)$$

In (1) and (2), the lift and drag coefficients are

$$C_l = \sin\alpha\cos\alpha, \quad (3)$$
$$C_d = \sin\alpha\sin\alpha. \quad (4)$$

However these coefficients are a function of only angle of attack α, and these are not affected by Reynolds number Re and the airfoil. These are constant with respect to change of Reynolds number and the airfoil. Hence the error between the simulation result and the experimental result was remained in [8]. For overcoming this problem, the lift force model is reconstructed considering Reynolds number.

The our flying robot with the cyclogyro wing rotates wings with about 7Hz. Thus the cyclogyro wing's Reynolds number is in the order of 10^4. According to Schmitz's experiment[9], the flat plate wing is superior in the aerodynamic characteristic to the air foil shape in Re=10000. Therefore we improve the lift force model in Fig. 5 based on the lift coefficient and the drag coefficient of the flat plate wing in Re=10000. The improved simulation model is validated by the simulation results calculated from the previous simulation model and the experimental results with the prototype.

A. Reconstruction of Lift Force Simulation Model

Fig.6 and Fig.7 show the lift and the drag coefficients in Re=10000. The lift and the drag coefficients are obtained as a function of the link's rotational angle θ. Therefore the lift and the drag in the link's rotational angle θ are calculated as

$$L(\theta) = \frac{1}{2}\rho v^2 S C_l(\theta) = \frac{1}{2}\rho(2\pi l_m f)^2 S C_l(\theta) \quad (5)$$
$$D(\theta) = \frac{1}{2}\rho v^2 S C_d(\theta) = \frac{1}{2}\rho(2\pi l_m f)^2 S C_d(\theta). \quad (6)$$

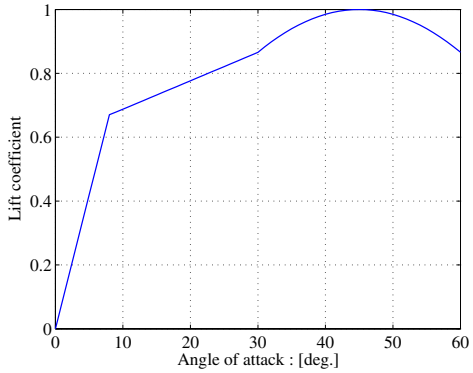

Fig. 6. Lift coefficient of flat plate in Re=10000[10].

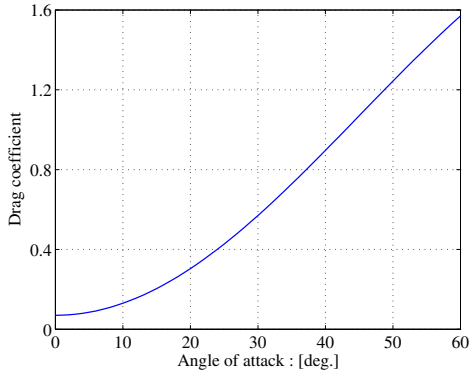

Fig. 7. Drag coefficient of flat plate in Re=10000[10].

Thus the vertical force $f_p(\theta)$ is represented as

$$f_p(\theta) = L(\theta)\cos(\theta+\pi) - D(\theta)\sin\theta = -L(\theta)\sin\theta - D(\theta)\sin\theta \quad (7)$$

from (5) and (6). The drag in (6) is also used for the calculation of the electric power in the power model. The vertical force $f_p(\theta)$ changes in a moment in the range of $0 \le \theta < 360$deg. since wings rotate with high frequency. Hence we assume that the lift force generated from a wing is the average of the vertical force $f_p(\theta)$ and all wings generate equal force. Then the total lift force generated by n wings is calculated as

$$F = \frac{n\int_0^{2\pi} f_p(\theta)d\theta}{2\pi}. \quad (8)$$

B. Validation of New Lift Force Simulation Model

The reconstructed simulation model is validated through the experiment using the prototype. The evaluation function J for validation is defined as

$$J = \frac{1}{m}\sum_{k=1}^{m}\frac{|Ve_k - Vs_k|}{Ve_k}\times 100. \quad (9)$$

In (9), Ve is the total lift force in the experiment generated by the prototype, Vs is the total lift force calculated by the simulation model and m is the number of experimental

results. The simulation model with smaller J represents the behavior of the prototype better.

Fig.8 shows the experimental results and the simulation results for two kinds of wing sizes, i.e., single chord wing ($w_c = 50$ mm) and double chord wing ($w_c = 100$ mm). The values of the evaluation function J in Fig.8 are shown in TableI. The evaluation function J of new simulation model gets about 18% smaller than that of previous model with single chord wing. On the other hand, the evaluation function J with double chord wing gets about 8% smaller. This means that the new simulation model has better simulation performance than previous model.

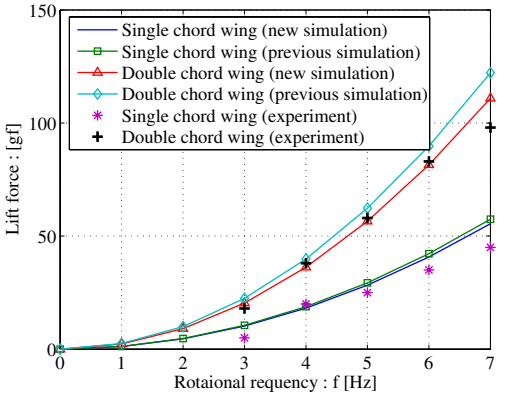

Fig. 8. Comparison between wing chord 50mm wing and 100mm wing.

TABLE I

COMPARISON OF EVALUATION FUNCTION J IN FIG.8.

	chord 50mm	chord 100mm
previous simulation model	36.58	17.55
new simulation model	18.82	9.68
difference between previous model and new simulation model	17.76	7.87

As mentioned before, the eccentric distance is the peculiar design parameter in the variable attack angle mechanism. Fig.9 and Fig.10 show the simulation and experimental results for some eccentric distances e (e=15mm, 20mm, 25mm and 35mm). The values of the evaluation function J in these results are shown in TableII. In all cases, the evaluation function J is reduced drastically and, the significant improvement of the simulation model is verified from TableII.

The simulation results by the reconstructed simulation model agree better with the experimental results than the simulation results of the previous model. Therefore, it is validated that the new simulation model is superior to the previous simulation model.

IV. DEVELOPMENT OF FORCE DIRECTION CONTROL MECHANISM

A. Force Direction Control Mechanism

The variable attack angle mechanism has two center points of rotation, that is, the center of rotation and the eccentric

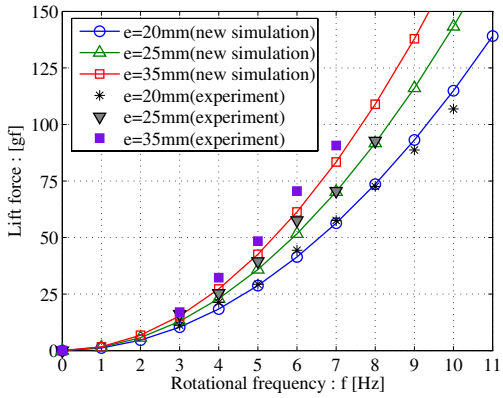

Fig. 9. Experiment and simulation results calcurated from new simulation model.

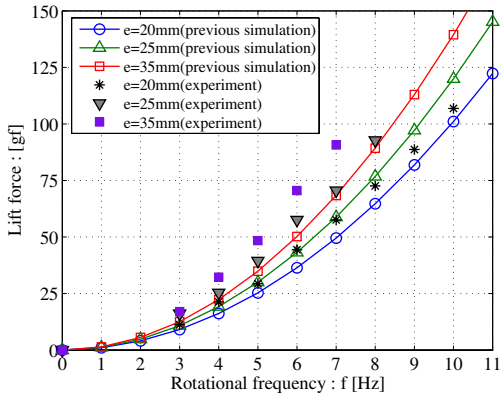

Fig. 10. Experiment and simulation results calcurated from previous simulation model.

point in Fig.11. The direction of the generated force is determined by the relative position of these points, i.e., the eccentric angle θ_p. The center shaft is set through the center of rotation, on the other hand the eccentric shaft is set through the eccentric point.

Fig.12 shows the design of the force direction control mechanism. The constructed prototype mechanism is also shown in Fig.12. Main links are driven by the main motor through the pinion and the main link gear. Note that the center shaft does not rotate by main motor, because the main link is independent of the rotation of the center shaft by the influence of the ball bearing. On the other hand, the center shaft gear and the eccentric arm are fixed on the center shaft. The center shaft and the eccentric arm are driven by the

TABLE II

COMPARISON OF EVALUATION FUNCTION J IN FIG.9 AND FIG.10.

eccentric distance	20mm	25mm	35mm
previous simulation model	9.15	19.39	29.17
new simulation model	5.18	3.70	13.55
difference between previous model and new simulation model	3.97	15.69	15.62

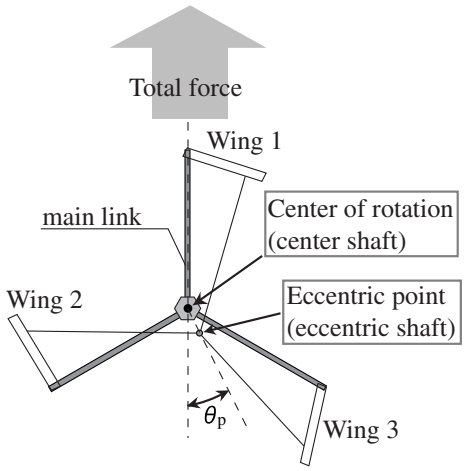

Fig. 11. Total force direction and two center points in variable attack angle mechanism.

servomotor mounted on the main motor through the servo gear. We can control the eccentric angle θ_p and the direction of the total force in Fig.11 by using this mechanism. The prototype has the following parameters and specifics.

- main link length : 200mm
- sub link length : 205mm
- eccentric distance : 10mm
- distance between links : 40mm
- main motor : 40W DC motor
- main motor weight : 132g
- servomotor weight : 15.6g
- servomotor torque : 4.8V 3.6kg-cm
- servomotor size : W26.2mm $\times$ D13mm $\times$ H31mm
- operating travel : 120deg.

B. Validation of New Mechanism

This section presents the validation of the force direction control mechanism through the experiment with the prototype shown in Fig.12. The mounted servomotor has 120deg. operating travel, thus, the control range is set in the eccentric angle from 0deg. to -120deg. in this prototype. The experimental system is shown in Fig.13 and Fig.14. The prototype with one rotor is fixed vertically on the 3D piezoelectric sensor, and the generated force is measured by this sensor. X-axis and y-axis are defined parallel to the piezoelectric sensor surface as shown in Fig.13. The direction of the generated force is calculated from measured x-axis and y-axis forces.

Fig.15 shows the step response of the force direction and the x-axis force and the y-axis force to the eccentric angle from 0 to -120deg.. The force direction follows the change of the eccentric angle. When the eccentric angle is changed, the x-axis force and the y-axis force change with a little delay because of the time-lag of the aerodynamic response.

Fig.16 shows the response of the force direction and the x-axis force and y-axis force to the sine curve of the eccentric angle. The x-axis force and y-axis force change in response to the change of the eccentric angle. The force direction

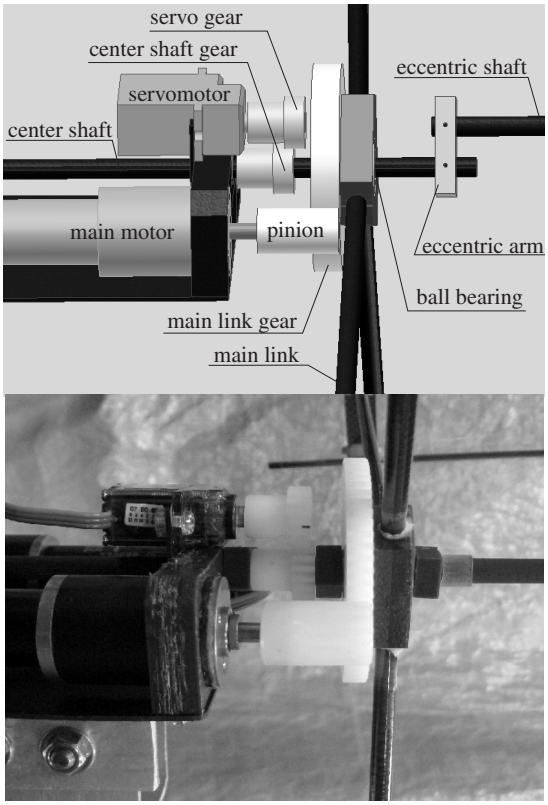

Fig. 12. Design and prototype of force direction control mechanism.

changes along the sine curve of the eccentric angle. These results show that the generated force can be controlled by the developed new mechanism.

The force direction coincides with the change of the eccentric angle well during increasing the eccentric angle. However during decreasing eccentric angle, small differences between the force direction and the eccentric angle are observed. The main reason of the difference is the relation between the drive direction of the eccentric angle and the wing rotational direction. The wing rotation is independent of the rotation of the center shaft because of the existence of ball bearing, but the remaining friction has an effect on the behavior of the eccentric angle. When the eccentric angle and the wings move in the same direction, the friction by the rotation is low. Contrary, when the eccentric angle and the wings move in the reverse direction, the friction by the rotation is high. This is why differences between the force direction and the eccentric angle are observed in Fig.16. However, enough tracking performance is achieved.

V. CONCLUSIONS

This paper has discussed the improvement of the simulation model and the development of the new mechanism of the flight control for the flying robot with the cyclogyro wing. The lift force model in the simulation model for flying robot with cyclogyro wing has been reconstructed in consideration of Reynolds number to improve the accuracy of the model. The constructed model has been verified through

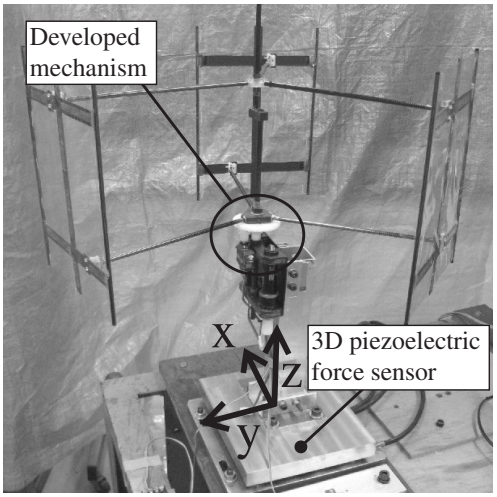

Fig. 13. Prototype and definition of x, y and z-axis on piezoelectric sensor.

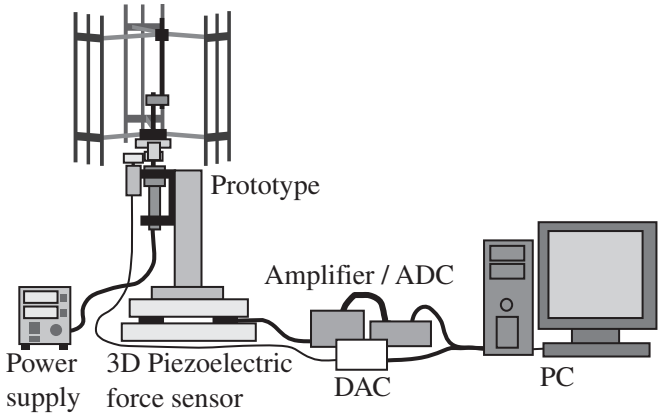

Fig. 14. Experimental system for validation.

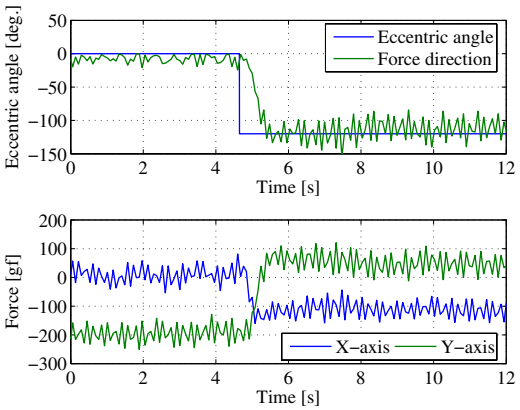

Fig. 15. Response of force direction to step input.

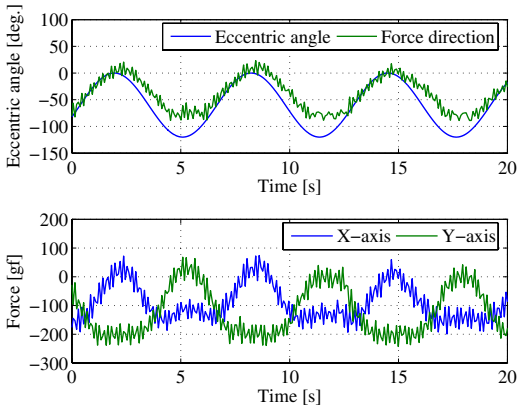

Fig. 16. Response of force direction to sine curve input.

the experiments using the prototype including changes of two design parameters, that is, the wing chord and the eccentric distance. In all validation experiment, the values of the evaluation function J calculated by the new simulation model are about 15% lower than the previous simulation model's results. The accuracy improvement of the simulation model has been verified by these results.

Moreover the new control mechanism of the direction of generated force has been developed. The developed mechanism has been validated by experiment with prototype. The measured force direction has followed the change of the eccentric angle, thus the utility of the developed mechanism has been verified by the experimental results. This mechanism is necessary for the flight control in our future work.

REFERENCES

[1] P. Rudol, M. Wzorek, G. Conte and P. Doherty, Micro Unmanned Aerial Vehicle Visual Servoing for Cooperative Indoor Exploration, Proc IEEE Aerospace Conference, Big Sky, MT., Mar., pp.1-10, 2008.

[2] A. Ryan, M. Zennaro, A. Howell, R. Sengupta and J.K. Hedrick, An overview of emerging results in cooperative UAV control, Proc IEEE Conference on Decision and Control, Bahamas, vol.1, Dec., pp.602-607, 2004.

[3] S.M. Ettinger, M.C. Nechyba, P.G. Ifju, and M. Waszak, Vision-guided flight stability and control for micro air vehicles, Advanced Robotics, Vol.17, No.3, pp.617-640 (2003)

[4] Q. Truong, Q. Nguyen, H. C. Park and N. S. Goo, The dynamic characteristics of LIPCA and its application for mimicking insect flapping motion, Proc IEEE/RSJ International Conference on Intelligent Robots and Systems, Nice, Sep., pp.131-136, 2008.

[5] M. Motamed and J. Yan, A Reinforcement Learning Approach to Lift Generation in Flapping MAVs: Experimental Results, Proc IEEE International Conference on Robotics and Automation, Roma, Apr., pp.748-754, 2007.

[6] The Cyclogyros:Planned paddle-wheel airplanes, http://www.dself.dsl.pipex.com/MUSEUM/TRANSPORT/cyclogyro/cyclogyro.htm

[7] Tanaka, K., Suzuki, R., Emaru, T., Higashi, Y. and Wang, H. O., Development of a Cyclogyro-Based Flying Robot With Variable Attack Angle Mechanisms, *IEEE /ASME Transactions on Mechatronics*, Vol.12, Issue 5, (2007-10), pp.565–570.

[8] Y. Higashi, K. Tanaka, H. Ohtake and Hua O.Wang, Construction of Simulation Model of a Flying Robot with Variable Attack Angle Mechanism, International Conference on Intelligent Robot and Systems, San Diego, CA, USA, Oct, 2007.

[9] R. T. Jones, S. Tuge and S. Asou, Wing Theory, The Nikkan Kogyo Shimbun, Ltd., p.40-45, 1993.

[10] M. Okamoto, Lift Characteristics for Small Size Model Plane, Proc The 1st Sky Sports Symposium, Tokyo, Dec., 1995.